Acta Materialia 216 (2021) 117110

Contents lists available at ScienceDirect

Acta Materialia

journal homepage: www.elsevier.com/locate/actamat

Full length article

# How grain boundary characteristics influence plasticity close to and above the critical temperature of ultra-fine grained bcc Ta2.5W

J. Kappacher[a,*], O. Renk[b], D. Kiener[a], H. Clemens[a], V. Maier-Kiener[a]

[a] Department of Materials Science, Montanuniversität Leoben, Leoben, Austria
[b] Erich Schmid Institut of Materials Science, Austrian Academy of Science, Leoben, Austria

ARTICLE INFO

*Article history:*
Received 4 March 2021
Revised 25 May 2021
Accepted 16 June 2021
Available online 29 June 2021

*Keywords:*
Nanocrystalline metals
Grain-boundary structure
Portevin-Le Chatelier effect
Thermally activated process
Nanoindentation

ABSTRACT

Dislocation-grain boundary interaction is widely accepted as the rate-controlling process for ultra-fine grained bcc metals in their high temperature deformation regime above the critical temperature. However, the influence of different types of grain boundaries remains widely unexplored so far. To this end we present here an advanced high temperature nanoindentation study on Ta2.5W specimens consisting of two distinctively different grain boundary types, but with similar submicron average spacing. While one set of samples consisted of a predominant fraction of high-angle boundaries, the second set contained mainly low-angle boundaries. Fully recrystallized samples served as a coarse grained reference batch. Using advanced nanoindentation at elevated temperatures up to 823 K, we find a temperature invariant hardness in the case of the low- and a strongly pronounced temperature dependence for the high-angle grain boundary samples. This underlines the importance of grain boundary diffusivity for the predominant process of interfacial stress relaxation. Pronounced interaction of dislocations with oxygen impurity atoms was observed from 473 to 773 K for the coarse grained microstructure, yielding serrated flow as an indicator for a Portevin-Le Chatelier effect up to 573 K. Both grain boundary types showed a significant influence to the dislocation-impurity interaction, whereby the high-angle grain boundaries suppress discrete flow characteristics.



## 1. Introduction

Over the last decade, modern technologies such as microelectronics, thin film technology or improved structural applications have led to an increased demand of materials with confined microstructure and architectures in the sub-micrometer regime. Already in the last century Hall and Petch [1,2] found that with decreasing grain size the strength of a material can be improved. In recent years this phenomenon was intensively studied for ultra-fine grained (ufg) face-centered cubic (fcc) as well as body-centered cubic (bcc) metals [3–6]. The fundamental understanding of plasticity for conditions where interfaces govern the increasing strength of materials is hence of vital interest for academic and industrial research.

In the case of dislocation controlled plastic deformation, the contribution of a single dislocation includes at least three mechanisms: nucleation, glide and storage or annihilation [7]. The slowest of these mechanisms, which usually depends on the activation energy, controls the overall plasticity and becomes the rate controlling process [8]. It is generally accepted that in a bcc lattice dislocation plasticity below the so-called knee-temperature or critical temperature, $T_K$, is controlled by a kink-pair mechanism [9,10]. Due to their complex core structure [11,12] screw dislocations in bcc metals exhibit a reduced mobility compared to edge dislocations [13,14]. As such, at low homologous temperatures these materials show a strong temperature-dependence of strength. The rate controlling process is the nucleation of double kinks [15]. For somewhat elevated temperatures, the double kinks become thermally activated, until above $T_K$ screw and edge dislocations exhibit the same mobility and the materials strength becomes athermal. In this high temperature (HT) regime dislocation motion is controlled by obstacle-controlled dislocation glide such as cutting of forest dislocations, analogous to coarse grained (cg) fcc metals [16,17].

Reducing the grain size of bcc metals to the ufg regime increases the athermal strength contribution and consequently the strain rate sensitivity of ufg bcc metals is lower compared to their cg counterparts [4,16,18,19]. This is attributed to an increased amount of long-range obstacles for dislocation motion provided by grain boundaries, while the contribution of the local Peierls barrier to the overall plasticity is reduced [18,20,21]. Despite these gener-

* Corresponding author.
*E-mail address:* johann.kappacher@unileoben.ac.at (J. Kappacher).

https://doi.org/10.1016/j.actamat.2021.117110

ally accepted findings, the rate controlling processes of bcc metals at the submicron scale remain intensively investigated. While several studies find that below $T_K$ deformation is still controlled by kink-pair formation for grain sizes or single crystal sample dimensions down to ~150 nm [16,22–24], some experiments and simulations at even smaller scales indicate a change of the rate controlling processes and a diminishing role of screw dislocations [25–28].

Contrarily to cg bcc metals, in ufg microstructures the rate-dependence of plastic deformation is reported to increase above a certain temperature. This indicates that dislocation-grain boundary interaction, facilitated by the refined microstructure, contributes increasingly towards the dominating deformation mechanism [16,18], in accordance with earlier reports on ufg fcc metals [29]. This critical temperature is at ~0.2 of the melting temperature, thus the temperature regimes for thermal activation of dislocation-grain boundary interaction and kink-pair formation may partly overlap, depending on the grain size of the ufg material [18,19]. For example, it was shown that alloying of W with Re can shift the increasing strain rate sensitivity towards higher temperatures, in accordance with the changed grain boundary diffusivity [30].

The kinetics, represented by the relaxation time $\tau$, of these dynamic recovery processes at grain boundaries, *i.e.* thermally activated accommodation of lattice dislocations within grain boundaries [31] can be described as follows [32,33]:

$$\tau = A\frac{k_B \cdot T \cdot s^3}{G \cdot \Omega \cdot D_{GB} \cdot \delta} \quad (1)$$

Apart from material constants such as the shear modulus, $G$, the atomic volume, $\Omega$, and the boundary width $\delta$; the absolute temperature, $T$, and fundamental constants such as a prefactor, $A$ (about 1/200 for severely deformed nanostructures [32]), and the Boltzmann constant, $k_B$, $\tau$ solely depends on the boundary diffusivity $D_{GB}$ and the spreading distance $s$, which is restricted to the grain size as an upper limit. Different types of grain boundaries exhibit a changed boundary diffusivity. That following, it was shown that low-angle grain boundaries provide a higher thermal stability compared to their high-angle counterparts, arising from reduced interfacial energies and diffusivities [34,35]. Renk *et al.* [36] recently demonstrated that the type of grain boundaries in nanostructured fcc Ni strongly affects the temperature dependent plasticity. While for the more diffusive high-angle grain boundaries properties obey a distinct temperature dependence, low-angle grain boundaries behave rather athermal over a wide temperature range. Different to nanostructured fcc metals, no study regarding the influence of the grain boundary type on the temperature-dependent strength currently exists for bcc metals at elevated temperatures. A lack of experimental data in this field is surprising, as several theoretical investigations highlighted the importance of the grain boundary misorientation angle (*i.e.* the grain boundary type) on the mechanical properties of bcc metals [37–39], and the materials are of importance for industrial application.

Since bcc refractory metals are commonly used as high temperature structural materials it is of urgent importance to understand the plastic deformation behavior above the knee-temperature, where deformation is found comparable to fcc metals. This is in particular true for high-performance nanostructures and the role of the respective grain boundary type. Therefore, Ta2.5W was chosen and analyzed in varying microstructural conditions. Comparing the temperature dependence of mechanical properties between a cg microstructure with ufg conditions, mainly consisting of either high-angle or low-angle grain boundaries, allows for careful analysis of the influence of different grain boundary misorientation angles on plasticity in bcc metals. As Ta is known for its sensitivity to interstitial impurities [40], it is of further interest, how the different types of grain boundaries affect the interaction of dislocations with interstitials and/or grain boundaries.

## 2. Experimental

Technically pure Ta2.5W (all chemical compositions given in wt.%) was received from Plansee SE (Reutte, Austria). A chemical analysis for interstitial impurities revealed a concentration of $<$ 5 ppm C, $<$ 2 ppm H, as well as 19±1 ppm N and 20±1 ppm O. The alloy Ta2.5W was selected as a model material for several reasons: due to the high melting point, $T_m$, of Ta, paired with a low $T_K$ [41–43], there is a rather large temperature regime, where kink-pairs are fully thermally activated but the microstructure is still thermally stable. Due to the rather low $T_K$ of Ta, compared *e.g.* to W, it can be rather well deformed via high pressure torsion (HPT) at room temperature, and thus microstructural saturation can be conveniently obtained [44]. Alloying with W serves to increase the thermal stability of the ufg microstructures at elevated temperatures [30]. To reach a recrystallized, cg (labeled CG) microstructure as a reference the sample was annealed for 2 h at 1773 K in a high vacuum furnace (HTM Reetz GmbH, Berlin, Germany). Two ufg structures with a deliberate change of the grain boundary type, but a rather equal spacing were synthesized to elucidate the differences in the thermomechanical response, one sample mainly consisting of grain boundaries with high-angle character (*i.e.* misorientation angle $\theta > 15°$) and a second one with mainly low-angle grain boundaries (*i.e.* $2° < \theta < 15°$), labeled as HAGB and LAGB, respectively. For the HAGB sample, discs of 8 mm diameter and 1 mm height were monotonously deformed via HPT [45] at ambient temperature for 10 rotations at a rotational speed of 0.2 rpm and a nominal pressure of 7.8 GPa. To create samples with LAGBs and a cell size in the sub-micrometer range cyclic high pressure torsion (CHPT) [46,47] was applied. Therefore, recrystallized Ta2.5W samples (1773 K, 2 h) with 10 mm diameter and 1 mm height were cyclically deformed at a 5° twist angle for five cycles. The rotational speed was again 0.2 rpm and the applied nominal pressure 5.1 GPa.

To ensure microstructural stability, *i.e.* to anticipate recovery or slight grain growth in the case of the HAGB sample, annealing for 2 h at 773 K was conducted in vacuum prior to mechanical testing. Microstructural investigations were performed in radial direction (RD) of the discs at a radius of 3 mm. The LAGB sample was microstructurally investigated in tangential direction (TD) of the sample and the chosen radius for further experiments was 4.5 mm.

For microstructural characterization as well as nanoindentation experiments the samples were carefully mechanically ground and polished. To remove any remaining deformation layer a final chemical polishing step was carried out with a 1:1 mixture of OP-S (Struers GmbH, Willich, Germany) and 5% KOH in $H_2O$. To reveal the microstructure of the CG sample back-scattered electron (BSE) images were taken on a Tescan Clara scanning electron microscope (SEM) (Tescan, Brno, Czech Republic) at 15 kV and the grain size was determined by means of line-intersection method. For the samples with submicron sized grains, microstructural imaging was received by an electron back-scatter diffraction (EBSD) setup from Bruker Nano GmbH (Berlin, Germany) equipped in a LEO 1525 field emission SEM (Carl Zeiss Microscopy GmbH, Jena, Germany) at 20 kV. Misorientation angles between adjacent grains were analyzed using the standard software package OIM analysis 7 from EDAX Inc. (Mahwah, NJ).

In order to investigate the mechanical properties, high temperature nanoindentation experiments were performed on an InSEM-HT nanoindenter from Nanomechanics Inc., KLA (Oak Ridge, TN) in axial direction (AD) of the samples. The system is equipped with a continuous stiffness measurement unit, superimposing a si-

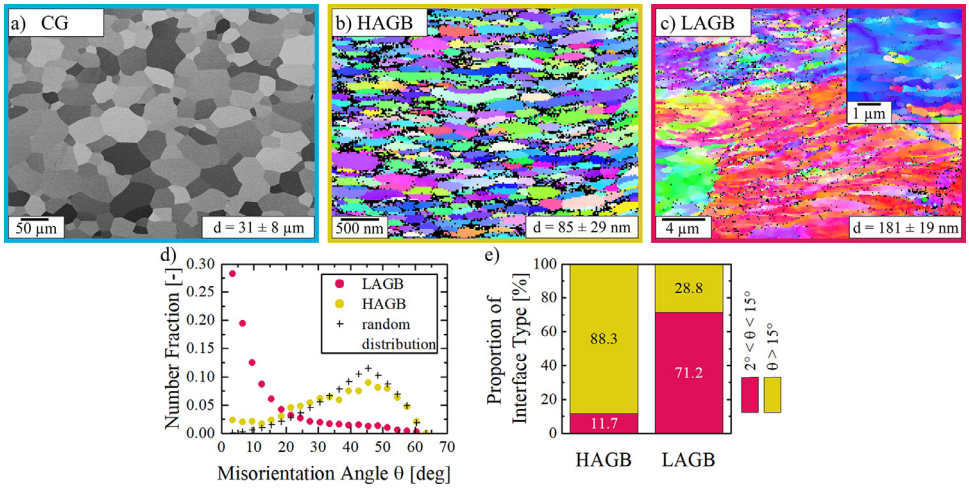


**Fig. 1.** Microstructure of the investigated Ta2.5W samples: a) BSE image of the CG condition; b) and c) EBSD images of the HAGB and LAGB sample, respectively. The misorientation distribution of the HAGB and LAGB samples and the according boundary fractions are displayed in d) and e).

nusoidal force signal with 100 Hz and a displacement amplitude of 2 nm to determine the contact stiffness continuously over indentation depth. For the CG and HAGB samples a WC, while for the LAGB sample a SiC Berkovich tip (both Synton MDP, Nidau, Switzerland) were used. The nanoindenter is installed in a Tescan Vega3 SEM (Tescan, Brno, Czech Republic) under high vacuum conditions ($< 10^{-4}$ mbar), allowing precise indent positioning as well as preventing high temperature oxidation of tip and sample. A tip temperature calibration was carried out by direct indentation into a thermocouple, as reported by Wheeler and Michler [48]. A stabilization time of approximately 2 h is required before the HT nanoindentation experiments to ensure low thermal drift for reliable data extraction. Area function and frame stiffness were obtained by room temperature (RT) indentation of fused quartz according to the analysis of Oliver and Pharr [49]. To follow any possible degradation of the tip after every sample testing series, additional indentations on fused quartz were performed at RT.

In order to obtain hardness, $H$, and Young's modulus, $E$, constant indentation strain rate experiments [50] were performed at $\dot{P}/P = 0.1\ s^{-1}$. The obtained values are averaged at an indentation depth of 700 to 800 nm for the CG sample and, due to the higher hardness and hence lower maximum indentation depth between 400 and 500 nm for LAGB and HAGB samples. Additional nanoindentation strain rate jump tests, as introduced by Maier *et al.* [51], with an abrupt change in strain rate by an order of magnitude to $\dot{P}/P = 0.01\ s^{-1}$ for at least 100 nm and finally switching back to $\dot{P}/P = 0.1\ s^{-1}$, were executed. At least ten valid indentation experiments were performed for every sample, temperature and test protocol. From the instantaneous hardness response [21] in respect to the changed indentation strain rate, the strain rate sensitivity, $m$, and the apparent activation volume, $V^*$, can be calculated according to Eqs. 2 and 3:

$$m = \frac{\partial(\ln(H))}{\partial(\ln(\dot{\varepsilon}))} \tag{2}$$

$$V^* = \frac{C^* \cdot \sqrt{3} \cdot k_B \cdot T}{m \cdot H} \tag{3}$$

with $C^*$ being a constraint factor of 2.8. $V^*$ is commonly normalized to the cubed Burgers vector, $b^3$, to facilitate comparison between different materials.

## 3. Results

### 3.1. Microstructure

In Fig. 1 the microstructure of the three investigated Ta2.5W samples, including statistical evaluation of the grain boundary characteristics, are presented. A BSE image of the recrystallized CG sample reveals globular equiaxed grains with an average diameter of 31±8 µm (Fig. 1a). Due to the large grain size compared to the maximum indentation depth of 900 nm, deformation is mainly governed by single crystalline behavior with diminishing influence of any sort of grain boundary. The inverse pole figure maps obtained by EBSD of the HAGB sample (Fig. 1b) exhibit typical HPT-deformed grains with an elongation in TD. The decisive grain diameter (small dimension) in AD was determined by the line-intersection method to be 85±29 nm, with the majority of grain boundaries being of high-angle character (*i.e.* $\theta > 15°$, Fig. 1e). The distribution of the misorientation angle (Fig. 1d) was found to be close to the random distribution. In Fig. 1c an overview of the microstructure of the LAGB sample is presented including an inset taken at higher magnification. Due to the CHPT deformation the subgrains are again elongated, with an average resolved cell size of 181±19 nm in the small dimension. At the chosen radius of 4.5 mm the proportion of LAGBs ($2° < \theta < 15°$, Fig. 1e) was more than 70%, which is also evident from the misorientation distribution in Fig. 1d.

### 3.2. Constant indentation strain rate experiments

The measured hardness over testing temperature for the three different samples is illustrated in Figs. 2a-c. The RT hardness values are 6.28±0.02, 4.63±0.14 and 2.81±0.07 GPa for the HAGB, LAGB and CG samples, respectively. The differences can be directly linked to an increased strength due to grain refinement. The observed evolution of hardness over temperature is significantly dependent on the different microstructures.

The HAGB sample (Fig. 2a) revealed a continuous decrease of hardness to 5.38±0.08 GPa up to 523 K. Between 573 and 723 K an increased hardness compared to the monotonous decrease can be observed with a peak of 5.89±0.04 GPa at 623 K. At the maximum testing temperature of 823 K the hardness was 4.46±0.08 GPa, while the RT hardness after this testing sequence was with 5.79±0.04 GPa lower than the as-prepared state, indicating thermally induced grain growth.

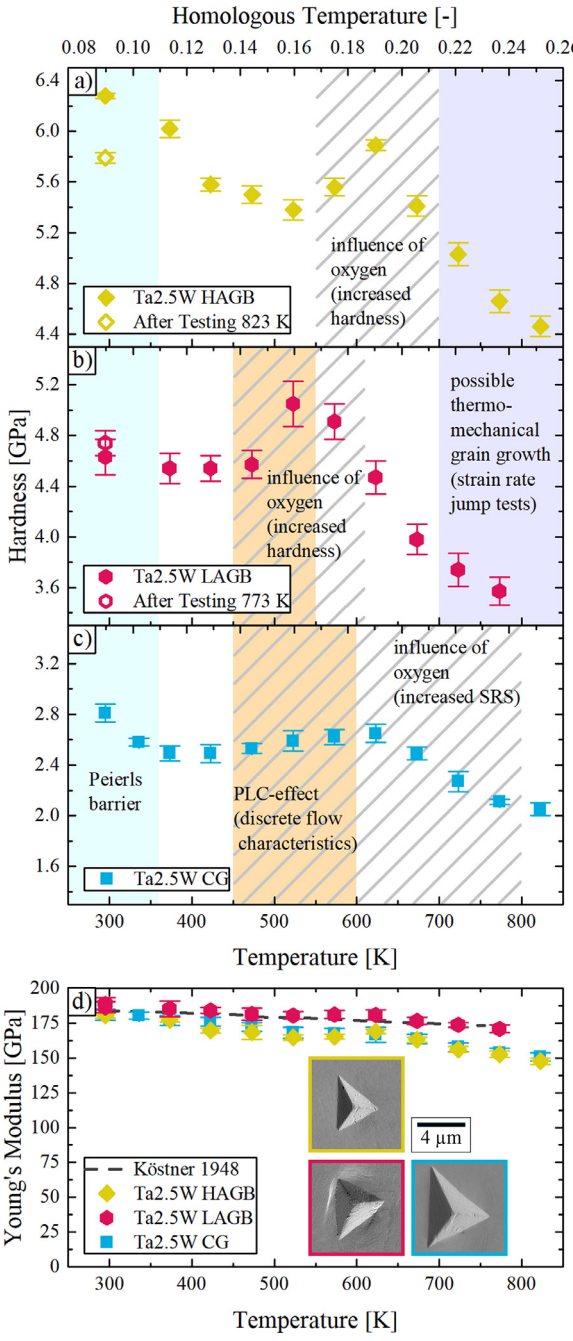


**Fig. 2.** Evolution of hardness over temperature for the three different microstructures: a) HAGB, b) LAGB and c) CG. In d) the measured Young's modulus is plotted over temperature in addition to literature values [52]. The insets show residual indents at RT (see text).

In contrast to the pronounced temperature sensitivity of the HAGB sample, probing LAGBs (Fig. 2b) revealed a temperature invariant hardness up to 473 K. An increased hardness compared to the general trend can again be observed between 523 and 623 K, with a peak of 5.05±0.18 GPa. At 773 K a hardness of 3.57±0.11 GPa was detected, while after the maximum testing temperature the RT hardness (4.74±0.10 GPa) slightly increased, although within standard deviation. The slightly higher scatter in the LAGB data, represented by a higher standard deviation of the measured values compared to the HAGB or CG sample can be assumed as a result of the less homogenized microstructure when compared to the cg behavior or the saturated grain size of the HAGB samples, as the size and shape of the developed dislocation boundaries depends on the crystallographic grain orientation.

The CG sample in Fig. 2c exhibits a strong temperature dependence of hardness up to 373 K (0.11 $T_m$). A further increase of the testing temperature results in an athermal hardness response (2.49±0.07 GPa) up to 423 K. Between 473 and 723 K an increased hardness can be observed, with a peak of 2.65±0.07 GPa at 623 K. At 823 K a value of 2.05±0.05 GPa was measured, while the hardness after HT testing was found unchanged (2.83±0.07 GPa).

In Fig. 2d the observed Young's modulus over temperature is presented along with additional literature values [52]. From the RT values of 180.4±1.9, 186.2±3.9 and 180.9±4.1 GPa for the HAGB, LAGB and CG sample, respectively, a monotonous decrease can be observed over the whole testing temperature range. The LAGB sample exhibits steadily higher values compared to the CG or HAGB samples. A slightly increased pile-up behavior, as illustrated in the inset in Fig. 2d for remaining indents at RT was observed for the LAGB sample. While the impressions in the CG and HAGB samples were almost perfect triangles, the remaining indents on the LAGB sample reveal a convex deviation from the ideal indent shape. Observing the impressions of different testing temperatures did not reveal a significant change in the pile-up behavior with temperature.

During the loading sequence of constant indentation strain rate experiments discrete flow characteristics could be observed in the CG sample from 473 to 573 K. Due to the intrinsically load controlled nature of the InSEM-HT system this behavior manifests as regular bursts in indentation depth and consequently drops in hardness, as shown in Fig. 3a. Such a behavior is typically associated with the Portevin-Le Chatelier (PLC) effect as a result of dislocations interacting with solute atoms. Although the effect is well described for macroscopic deformation experiments, detailed analyses via nanoindentation focused mainly on Al alloys so far [53–56]. Comparing the appearance of the hardness over indentation depth (Fig. 3a) for different temperatures indicate a strong temperature dependence of this mechanism. While for 473 and 523 K it is regular and periodic over the whole indentation depth, at 573 K the hardness drops occurred less regular at random indentation depth. The effect is qualitatively most pronounced at 523 K, showing the most prominent and rapid hardness drops. While non such behavior could be observed at any temperature for the HAGB sample (Fig. 3c), the LAGB sample showed a slightly periodically curvy flow at 523 K (Fig. 3b). Additionally, during the low indentation strain rate of $\dot{P}/P$= 0.01 $s^{-1}$ in the strain-rate jump tests, serrated flow could also be observed at 473 K. The events are, however, less pronounced compared to the CG material. For a better illustration, the temperatures where a PLC effect was observed are highlighted in orange in Figs. 2 and 3.

### 3.3. Nanoindentation strain rate jump tests

The results of the strain rate jump tests, strain rate sensitivity and apparent activation volume are plotted in Fig. 4 over temperature. At RT $m$-values of 0.014±0.001, 0.009±0.001 and 0.010±0.001 for the CG, HAGB and LAGB sample, respectively, were determined. For the CG sample towards $T_K$, the strain rate sensitivity decreases to 0.004±0.001 with increasing temperature at 373 K (around 0.11 $T_m$). As the testing temperature further increases a negative strain rate sensitivity can be observed (473 and 523 K), followed by a strongly rate sensitive strength regime between 623 and 773 K. At 823 K hardness is again almost strain rate independent with $m$ = 0.002±0.001. In the HAGB sample $m$ remains constant at 0.008±0.001 up to 523 K, followed by a steady increase as temperature rises up to the maximum testing temperature, where values of 0.040±0.006 were measured. The strain rate sensitivity of the LAGB sample continuously decreases to 0.003±0.001 at 423 K,

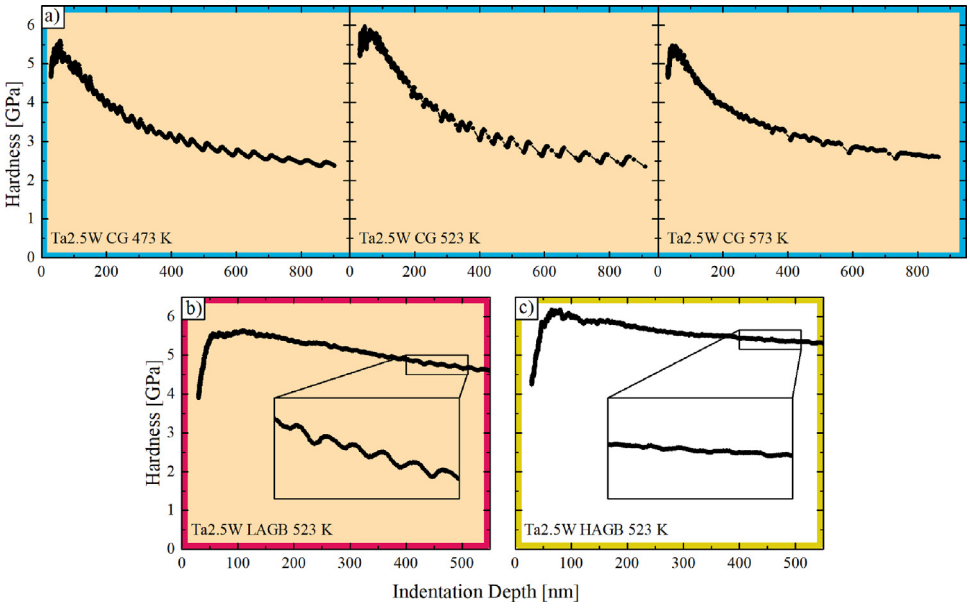


**Fig. 3.** Hardness over indentation depth for selected temperatures to illustrate the discrete flow characteristics of the PLC effect in a) the CG condition. For the ufg samples consisting mainly of b) LAGBs a slightly wavy flow can be observed at 523 K, while such a behavior could not be detected for the c) HAGB sample.

with a negative strain rate sensitivity at 473 K and constant values from 573 to 773 K between 0.014 and 0.019. After the maximum testing temperature, the HAGB sample reveals a slightly reduced strain rate sensitivity of 0.006±0.001 at RT, while the values for the LAGB and CG samples remained the same within the standard deviation.

The corresponding activation volume, as an indicator for the volume collectively involved in the rate controlling deformation mechanism [57], was found to be very similar at RT (21±3, 16±2 and 20±3 $b^3$ for CG, HAGB and LAGB, respectively). Note that no activation volumes were calculated for temperatures, where negative strain rate sensitivities were measured. The activation volume in the CG sample shows the strongest increase with temperature, reaching values of more than 100 $b^3$ at 373 K. Additionally, between 623 and 773 K lower values between 30 and 80 $b^3$ were observed. The HAGB sample exhibits the lowest increase with temperature, peaking at 523 K (35±6 $b^3$), followed by a continuous decrease towards 823 K, where a value of 15±3 $b^3$ was measured. The LAGB sample follows the trend of an increasing activation volume between RT and 423 K (107 $b^3$). Above 523 K values between 20 and 60 $b^3$ were determined. After high temperature nanoindentation the CG and LAGB samples exhibit an unchanged activation volume at RT, while for the HAGB sample a slight increase towards 25±5 $b^3$ was observed.

In Fig. 5 the evolution of hardness over indentation depth for representative strain rate jump tests are shown for the CG (a), LAGB (b) and HAGB (c) samples at different temperatures. While the change in strain rate by an order of magnitude develops in an instantaneous change in hardness for most of the presented curves, testing the HAGB sample at 723 K and higher temperatures results in a more transient behavior. Also the hardness after the change in strain rate back to the original value does not reach the same plateau as before the first jump. This is also true for the LAGB sample tested at 723 and 773 K. The change in strain rate also has a remarkable influence on the discrete flow characteristic caused by the PLC effect. In the CG sample, where such a behavior was observed during constant strain rate experiments from 473 to 573 K, the reduced strain rate results in a more pronounced serrated flow at 473 K, while at 523 and 573 K the hardness drops diminish. A similar behavior can be observed for the LAGB sample, where serrated flow is evident for low strain rates at 473 K, but not at the standard strain rate of 0.1 $s^{-1}$. The performance reverses again at 523 K, where a wavy hardness over indentation depth can be observed for 0.1 $s^{-1}$, while a smooth flow characteristic is visible for 0.01 $s^{-1}$.

## 4. Discussion

Upon comparing the plastic deformation behavior as a function of temperature between the cg microstructure, sampling a minor contribution from grain boundaries, with samples where the probed volume consists mainly of either high- or low-angle grain boundaries, it is evident that the type of grain boundary has a significant impact on the deformation behavior. Notably, the well matching Young's modulus over temperature and its accordance with literature [52] confirms the validity of our data. Slightly increased modulus values in the case of the LAGB sample are most probably related to the different indenter materials used, as a varying temperature dependence of the Young's modulus of the tip material as well as general inaccuracies of the values at RT can cause significant errors in the measured Young's modulus of the investigated material [58]. The higher values could also be influenced by the observed slight pile-up behavior in the case of the LAGB sample, resulting in a overestimation of hardness as well as elastic modulus [59].

### 4.1. Dislocation – solute atom interaction

The mechanical properties of bcc metals in general and the reactive Ta in particular, are sensitive to interstitial impurities such as O, N or C [40]. Internal friction experiments on Ta reveal a Snoek peak between 500 and 750 K [60,61], which was related to migration of O atoms leading to partial pinning of dislocations [62,63]. Such local atomic jumps can not only impede the movement of dislocations but also affect the stress relaxation by defect induced distortion [64]. In the temperature regime of the impurity-induced relaxation peak the hardness of the CG sample shows an anomalous increase with temperature (Fig. 2c) and an increased strain rate sensitivity (Fig. 4). Similar observations were made in macroscopic compression tests where an increased flow stress was observed between 600 and 800 K for technically pure Ta2.5W with

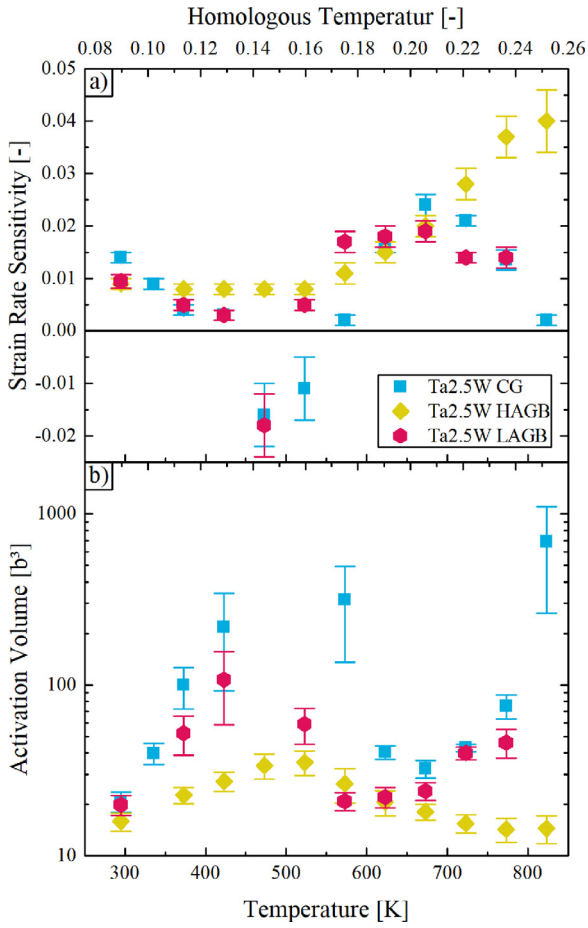


**Fig. 4.** Results of the strain rate jump tests: a) strain rate sensitivity and b) activation volume over temperature. For a negative strain rate sensitivity no activation volume was calculated.

53 ppm O [65]. Pink [66] reported an increased flow stress of Ta with 6 ppm O at 10% strain between 573 and 773 K. He further outlined, that a single impurity species may hinder the dislocation motion and hence increase the flow stress in two different ways: Either by forming Cottrell clouds or by a strain-induced ordering process related to the Snoek-effect. The rate-controlling step of the two mechanisms is different, hence they may occur at different temperature intervals. The former effect is, however, responsible for a serrated flow characteristic, as reported in [67] between 473 and 573 K. This strongly suggests that the uncommon increase of hardness with temperature is a result of thermally activated dislocation-impurity interactions.

It is generally accepted that the serrated flow behavior of the PLC effect originates from dynamic strain aging, *i.e.* thermally activated release of solute-decorated mobile dislocations, in conjunction with solute aging of forest dislocations [68,69]. In a certain temperature and strain rate range, mobile dislocations that are temporarily pinned by forest dislocations become occupied with sufficiently mobile solutes. A negative strain rate sensitivity can thus be observed, as the stress required to detach the solute-decorated dislocation is higher than keeping the dislocation in motion upon their release [70]. Hence, diffusion of the responsible solute atoms has to be high enough to age the pinned dislocations. Using a diffusion pre-factor, $D_0$ (0.0044 cm²/s), and an activation energy for diffusion, $E_A$, of 106.483 kJ/mol [71,72], the calculated diffusion coefficient for O in Ta is $1.02 \cdot 10^{-17}$ m²/s at 523 K. Other impurities, such as N or C have a several magnitudes lower diffusion coefficient [72,73]. For the substitutional alloying element W, the diffusion coefficient can only be extrapolated from experiments performed at much higher temperatures, however, this results in a value in the order of $10^{-39}$ m²/s at 523 K [74]. Estimating a diffusion path for O interstitials in Ta through $x = 2\sqrt{D \cdot t}$ for 1 s gives a value of 6 nm. This is well within the range of the deformation rate applied in the nanoindentation experiments, which increases linearly with displacement up to around 40 nm/s at an indentation depth of 800 nm. Hence it can be argued that the interaction of O impurity atoms with dislocation cause a PLC-like behavior in the CG Ta2.5W alloy.

Interestingly, the influence of O in the case of the ufg microstructure manifests different. Generalization of the influence of grain boundaries on the PLC behavior is difficult, as it is dependent on microstructure and (local) chemical composition, which, regarding the microstructure, strongly depends on material processing [55]. In Al-Mg alloys it was shown, that for AA5182 HPT deformation leads to a smooth load-displacement behavior during nanoindentation, while the same material exhibits serrated flow in the recrystallized condition [75]. Contrarily, ufg AA5754 shows pronounced discrete flow characteristics at low strain rates [76]. In the present study no PLC-effect could be observed in the case of the ufg HAGB sample, while for the LAGB sample a PLC effect is evident at 473 and 523 K, although less pronounced compared to the CG microstructural condition. As the drops in hardness require collective motion of dislocation avalanches [77], HAGBs may act as barriers, suppressing a serrated flow. It could be argued that for LAGBs the effect is attenuated, but slip transfer between adjacent subcells is still possible, resulting in the observed periodically curvy flow.

While the HAGB sample exhibits a peak hardness at the same temperature as the CG specimen (623 K), the temperature regime where hardness is obviously influenced by solute atoms is narrowed between 573 and 673 K. An increasing strain rate sensitivity with temperature is evident starting at 573 K, however, such a behavior is typical for ufg bcc metals above a critical temperature [16,18,30], indicating a thermally activated facilitation of dislocation-grain boundary interaction through diffusion processes. It can be assumed that an increased strain rate sensitivity caused by the thermally activated accommodation of lattice dislocations within grain boundaries overlaps with the dislocation-impurity interaction and hence no clear distinction between the two effects on the strain rate sensitivity can be made. Generally, the interaction of dislocations with impurities strongly depends on the diffusivity of the solute atoms, which in turn is enhanced through interfaces, such as grain boundaries, resulting in different temperatures where impurity effects occur. Another plausible explanation would be, that in the ufg microstructure impurity atoms preferably segregate towards grain boundaries, as even reported for other cg refractory metals [78]. Oxygen in particular has a strong tendency for grain boundary segregation in refractory metals [79]. The difference in the peak-hardness temperatures between the HAGB and LAGB sample could thus arise from a change in the O concentration in the grain interior due to different grain boundaries and the synthesis route. Conventional HPT deformation in case of the HAGB sample introduces large amounts of strain ($\varepsilon = 109$ at r = 3 mm) and the final grain size is a result of an equilibrium of generated and annihilated grain boundaries [80]. Already during this process grain boundaries can be enriched with solute atoms [81], in particular with interstitial elements [82]. In contrast to that, during cyclic HPT the material experiences significantly less plastic deformation ($\varepsilon_{acc} = 4.5$ at r = 4.5 mm). Subcell boundaries are introduced in large preexisting, recrystallized grains (compare Fig. 1c). A strain induced O decoration of these LAGBs to similar levels as for the HAGBs thus seems improbable. This situation is not expected to change during the heating sequence of the HT nanoindentation tests. While the absolute interfacial excess may change

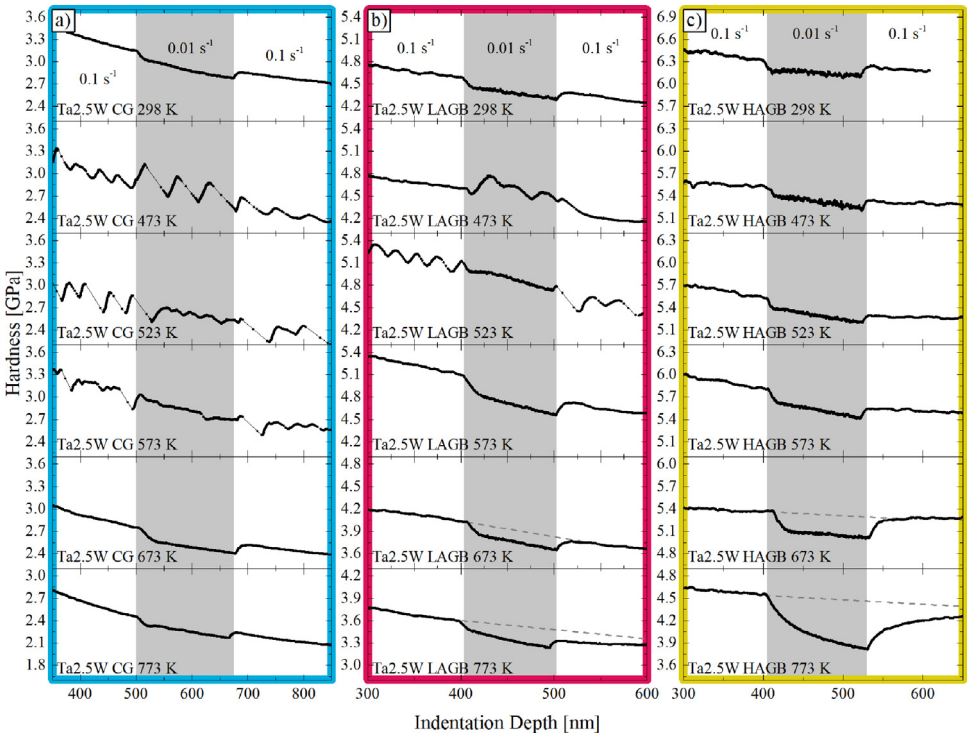


**Fig. 5.** Magnification of the hardness response due to a change in strain rate during the strain rate jump tests for a) CG, b) LAGB and c) HAGB samples at selected temperatures.

for both samples, this should not affect the differences discussed – except for special HAGBs, the interfacial excess after a thermo-mechanical treatment was always reduced for LAGBs compared to general HAGBs [83]. Therefore, the grain interior of the HAGB sample is expected to be depleted in O atoms compared to the LAGB sample, possibly causing an increased peak-hardness temperature. Such an argumentation is supported by an early work of Szkopiak [84], who investigated the strain aging behavior of the system Nb-O: RT tensile tests on prestrained and aged Nb samples revealed a shift of the maximum increase in the lower yield point, $\Delta\sigma_y$, towards longer aging times for lower O concentrations. Applied to our investigations this means that less O atoms within the grains cause a shift of the peak-hardness towards higher temperatures.

Finally, at the end of this section the question to be addressed is whether the 20 ppm of O derived from chemical analyses are sufficient to cause the observed effects, or if impurities were taken up during high temperature testing from the residual gas in the vacuum chamber. For enrichment of O within Ta2.5W two different steps need to be fulfilled: adsorption of molecules onto the sample and diffusion of the solved atoms towards a sufficient distance from the surface. Diffusion from the surface can be estimated from Eq. 4 [85]:

$$c(x) = c_R \cdot \mathrm{erfc}\left(\frac{x}{2\sqrt{Dt}}\right) \tag{4}$$

Here, $c(x)$ represents the concentration of a diffusing species at a distance $x$ from the surface, $c_R$ is the constant concentration at the surface, $D$ is the diffusion coefficient at a certain temperature and $t$ the time. Considering $D$ of O in Ta at the maximum testing temperature of 823 K ($7.67 \cdot 10^{-14}$ m²/s [72]) and an average annealing time of 3 h, an increase in the O content up to around 9% of the surface concentration $c(x)/c_R$ can be assumed at a distance of 800 nm from the surface. Thus, from a diffusion perspective an enrichment of O in the material is conceivable. Cowgill and Stringer [86] investigated the surface contamination of Ta with O for a variety of temperatures and pressures considering a Langmuir isotherm and reported a surface coverage of 20% at 823 K for a pressure of 67 mbar. It is further described that the surface coverage is linearly related to the applied pressure for a low pressure regime. Since in the current study the experiments were executed in vacuum below $10^{-4}$ mbar, almost six orders of magnitude lower compared to the investigations in [86], the O surface coverage of Ta can be assumed as negligible. Thus, the observed dislocation-oxygen interaction can be solely related to the initial O content in the material (20 ppm), also supported by the unchanged hardness of the CG sample after testing at 823 K.

### 4.2. Microstructural thermo-mechanical stability

The large fraction of grain boundaries makes ufg microstructures prone to grain growth already at comparably low homologous temperatures. Annealing the HAGB sample prior to HT nanoindentation at 773 K for 2 h ensures that pure thermally induced grain growth up to this temperature and annealing time can be neglected. Probing the sample at the maximum testing temperature of 823 K, however, results in grain growth, as can be derived from the reduced RT hardness (Fig. 2a) determined subsequently to the maximum testing temperature. Microstructural investigations of isochronally annealed (2 h) HAGB samples confirm this behavior (Fig. A1). A continuous increase of the decisive grain diameter in AD can be observed with increasing annealing temperature above 773 K. Representative for the HT nanoindentation experiments a grain size increase of 16% can be observed for a sample annealed at 823 K (average grain diameter 99 nm) compared to annealing temperatures of 773 K (average grain size 85 nm). The RT hardness of the LAGB sample after testing at the maximum temperature of 773 K demonstrates that measurements are conducted within the thermal stability limit of the microstructure.

However, grain boundary migration and hence grain coarsening can occur facilitated through applied stresses [87–89]. Thereby, grain growth can take place in the plastic deformation zone underneath the indenter even below the thermal stability limit [36,90].

In fact, observations on pure nanocrystalline Cu [91] suggest that mechanically induced grain growth is driven by the applied stress rather than diffusion-controlled at elevated temperatures. A necessary indicator for such a behavior can be derived from the hardness response over indentation depth during strain rate jump tests (Fig. 5). For a thermo-mechanically stable microstructure, the jump back to the initial strain rate should result in the same hardness level. If this is not the case, as indicated with grey lines in Fig. 5 for both HAGB and LAGB samples above 723 K, the microstructure underneath the indenter is prone to grain growth, explaining the observed reduced hardness above this temperature [36].

### 4.3. Regarding the rate-controlling deformation mechanisms

The temperature dependence of hardness of the CG sample (Fig. 2c) as well as the decreasing strain rate sensitivity and accordingly increasing activation volume indicate kink-pair formation as the rate controlling deformation mechanism below 0.11 $T_m$ [9,10]. Above 373 K hardness remains athermal, while the rate sensitivity is 0.003. An increasing activation volume with temperature can be interpreted with larger spreading of the kink-pairs due to thermal activation [18] while 100 $b^3$ at 373 K indicate a changing deformation mechanism towards dislocation-dislocation interaction [92]. It is worth noting that the low activation volumes between 623 and 773 K represent the strong influence of diffusion processes on the deformation behavior as described above. The homologous temperature of around 0.11 $T_m$ for thermal activation of the kink-pairs in Ta2.5W is relatively low compared to other bcc metals, where $T_K$ is reached around 0.20 $T_m$ [16,93]. This is in line with a double-kink formation energy, reported to be 0.74 eV for Ta, what is less than half the value of W (1.60 eV) [94]. A similarly low transition temperature was further experimentally confirmed by several authors [41,42,65]. The reduced hardness at 823 K compared to 423 K, where deformation is controlled by cutting of forest dislocation and the yield stress should be temperature independent, can be explained by dynamic dislocation interaction during indentation. Nanoindentation with a Berkovich indenter applies a representative strain of 7.16% [95]. Hence, for materials with a strong work hardening tendency, a significant contribution to the measured hardness values will originate from strain hardening [96]. As the testing temperature increases, the work hardening rate may decrease and thus the measured hardness value would be reduced although the yield point could remain the same. The work-hardening behavior of recrystallized Ta2.5W as derived from compression tests on macroscopic samples decreases significantly at these high temperatures, while the yield stress remains constant [67]. Hence, dynamic recovery is enhanced at 823 K, represented by decreasing hardness values.

The difference in the temperature- and strain rate-dependence of hardness regarding the HAGB and LAGB sample is striking. Below testing temperatures where an influence of O is evident, the HAGB sample exhibits a strong temperature dependence with a hardness decrease of around 0.9 GPa up to 523 K, whereas the LAGB sample behaves almost perfectly athermal. The microstructure is thermally stable in this temperature regime; hence this behavior can be solely related to the influence of the grain boundary character to the deformation mechanism. Notably, a kink-pair controlled deformation regime for the ufg microstructures could not be clearly identified from the hardness or flow stress over temperature. The results of the strain rate jump tests reveal a comparable behavior between the CG and LAGB sample, while the strain rate sensitivity in the case of the HAGB sample is unaffected between RT and 373 K. However, due to the lack of sufficient data points below $T_K$ the question regarding the dominating processes for the ufg samples in this deformation regime will not be addressed in this manuscript. Thus, the following discussion refers to temperatures exceeding 373 K. The activation volume of several 10 $b^3$ indicates dislocation-grain boundary interaction as the rate controlling step [16], *i.e.* plastic deformation is controlled by dynamic recovery processes at grain boundaries and grain boundary diffusion [29,31]. As described by Eq. 1 the relaxation time for these processes scale inversely with the grain boundary diffusivity. While no grain boundary diffusion data that distinguishes between LAGB and HAGB is available for Ta, diffusivity along grain boundaries in general is strongly dependent on the misorientation angle of the two adjacent grains [97–99]. For fcc Ni, where interfacial diffusivity is well investigated, the grain boundary diffusion coefficient for LAGBs is at least two orders of magnitude lower [35,36] and a similar trend can be assumed for Ta. Consequently, the reduced relaxation time in the case of HAGBs results in an increased thermal activation of dislocation-grain boundary interaction, reflected by the stronger temperature- and rate dependence of flow stress [36]. The increasing strain rate sensitivity above 573 K for both ufg samples indicates that the mechanism is thermally facilitated above this temperature. As dislocation-grain boundary interaction is a thermally activated process, part of the energy barrier can be overcome by mechanical work, see Eq. 5 [100]:

$$\Delta F^* = \Delta G^* + \tau^* \cdot V^* \tag{5}$$

Here, $\Delta F^*$ is the Helmholtz free energy to overcome the energy barrier, consisting of a thermal contribution, represented by the Gibbs free energy $\Delta G^*$ and an equivalent mechanical work $\tau^* \bullet V^*$, where $\tau^*$ is the resolved shear stress. While Eq. 1 only considers the thermal contribution to the relaxation time, the applied high shear stresses during nanoindentation of the ufg structures allow to surmount the activation energy for dislocation-grain boundary interaction below temperatures where the process is facilitated by thermal activation only [29,36]. This is in line with the difference in temperature dependent hardness for samples consisting mainly of HAGBs and LAGBs even below the temperature where strain rate sensitivity increases remarkably.

The results of the present study underline the importance of interfacial stress relaxation in the high temperature deformation regime of ultra-fine grained bcc metals. Comparison with nanostructured fcc metals of different grain boundary types [36] further confirmed that the rate-controlling deformation process is common for nanostructured metals of both crystal structures, namely accommodation of lattice dislocations within grain boundaries. Based on our present results, we underline the significance of kinetics for accommodation processes of dislocations at grain boundaries. This finding is of general nature and transferrable and should thus be considered for future materials developments in high-performance structural applications: A reduced temperature-sensitivity of strength combined with a higher thermal stability renders nanostructured bcc materials with LAGBs beneficial compared to HAGBs. This is in particular true for application temperatures close to the thermal stability limit. While processing routes still require improvements to synthesize these nanostructured bcc materials on a larger scale, our findings potentially open future research fields for improved grain boundary engineering.

## 5. Conclusions

High temperature nanoindentation was conducted on Ta2.5W in the recrystallized as well as severely deformed condition, with these samples consisting mainly of high- and low-angle grain boundaries, respectively. The goal of this research was to clarify how interfacial stress relaxation is affected by the grain boundary type in bcc metals in the high temperature deformation regime. From a comparison of the temperature- and strain rate-sensitivity of hardness the following conclusions can be drawn:

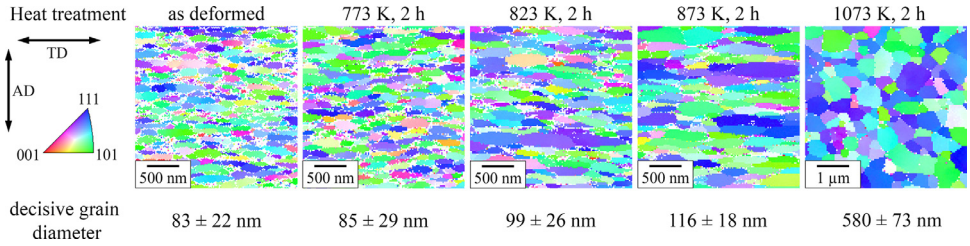


**Fig. A1.** Microstructural evolution of HAGB samples for different 2 h isochronal annealing experiments. The inverse pole-figure maps indicate grain grow above 773 K, supporting the interpretation of HT nanoindentation experiments at the maximum testing temperature.

- The differences in the behavior of HAGB and LAGB emphasizes the importance of interfacial stress relaxation and its dependence on boundary diffusivity. Our results strongly suggest that the high temperature deformation behavior in ufg bcc metals above the knee-temperature is controlled by accommodation of lattice dislocations within grain boundaries, a process that occurs mechanically driven at low homologous temperatures and accelerates by thermal activation above a certain critical temperature. Thus, the temperature- and rate dependence of hardness is strongly pronounced in samples consisting mainly of HAGB, while LAGB perform rather athermal and thus a lower strain rate sensitivity is evidenced.
- Between 473 and 773 K the flow stress of Ta2.5W is strongly affected by small amounts (20 ppm) of O dissolved in the crystal. From 473 to 573 K a Portevin-Le Chatelier effect with serrated flow characteristics is evident, while at higher temperatures the effect manifests in an increased hardness and strain rate sensitivity.
- The grain size and boundary character in the lower end of the ultra-fine grained scale have a significant impact on the dislocation-interstitial interaction, resulting in a shift of the temperature for which the flow stress is affected and suppression of discrete yielding in the case of HAGBs.

## Declaration of Competing Interest

The authors declare that they have no known competing financial interests or personal relationships that could have appeared to influence the work reported in this paper.

## Acknowledgements

The authors want to thank Plansee SE for providing the material. D.K. acknowledges funding by the European Research Council under Grant number 771146 (TOUGHIT). O.R. acknowledges funding from the Austrian Academy of Sciences via Innovation Fund IF 2019-37.

## Appendix

Figure A1

## References

[1] E.O. Hall, The deformation and ageing of mild steel: III discussion of results, Proc. Phys. Soc. B. 64 (1951) 747, doi:10.1088/0370-1301/64/9/303.
[2] N.J. Petch, The cleavage strength of polycrystals, J. Iron Steel I 174 (1953) 25–28.
[3] R. Fritz, V. Maier-Kiener, D. Lutz, D. Kiener, Interplay between sample size and grain size: single crystalline vs. ultrafine-grained chromium micropillars, Mater. Sci. Eng. A 674 (2016) 626–633, doi:10.1016/j.msea.2016.08.015.
[4] D. Wu, X.L. Wang, T.G. Nieh, Variation of strain rate sensitivity with grain size in Cr and other body-centred cubic metals, J. Phys. D. Appl. Phys. 47 (2014), doi:10.1088/0022-3727/47/17/175303.
[5] J. May, H.W. Höppel, M. Göken, Strain rate sensitivity of ultrafine grained FCC- and BCC-type metals, Mater. Sci. Forum. 503–504 (2006) 781–786, doi:10.4028/www.scientific.net/msf.503-504.781.
[6] Q. Wei, S. Cheng, K.T. Ramesh, E. Ma, Effect of nanocrystalline and ultrafine grain sizes on the strain rate sensitivity and activation volume: FCC versus bcc metals, Mater. Sci. Eng. A 381 (2004) 71–79, doi:10.1016/j.msea.2004.03.064.
[7] D. Caillard, J.-L. Martin, Thermally activated mechanisms in crystal plasticity, Pergam. Mater. Ser. (2003).
[8] J.W. Christian, The Theory of Transformations in Metals and Alloys, Newnes, 2002.
[9] B. Sestak, A. Seeger, Gleitung und Verfestigung in kubisch-raumzentrierten Metallen und Legierungen, Z. Met. 69 (1978) 195–202.
[10] A. Seeger, The temperature and strain-rate dependence of the flow stress of body-centred cubic metals: a theory based on kink-kink interactions, Z. Met. 72 (1981) 369–380.
[11] V. Vitek, Theory of the core structures of dislocations in body-centered-cubic metals, Cryst. Lattice Defects 5 (1974) 1–34.
[12] M.S. Duesbery, V. Vitek, Plastic Anisotropy in B.C.C. transition metals, Acta Mater. 46 (1998) 1481–1492 http://www.olympusmicro.com/primer/lightandcolor/birefringence.html.
[13] J.W. Christian, Some surprising features of the plastic deformation of body-centered cubic metals and alloys, Metall. Trans. A 14 (1983) 1237–1256 https://link.springer.com/content/pdf/10.1007/BF02664806.pdf.
[14] M. Tang, L.P. Kubin, G.R. Canova, Dislocation mobility and the mechanical response of B.C.C. single crystals: a mesoscopic approach, Acta Mater. 46 (1998) 3221–3235, doi:10.1016/S1359-6454(98)00006-8.
[15] M.S. Duesbery, W. Xu, The motion of edge dislocations in body-centered cubic metals, Scr. Mater. 39 (1998) 283–287, doi:10.1016/S1359-6462(98)00162-6.
[16] D. Kiener, R. Fritz, M. Alfreider, A. Leitner, R. Pippan, V. Maier-Kiener, Rate limiting deformation mechanisms of bcc metals in confined volumes, Acta Mater. 166 (2019) 687–701, doi:10.1016/j.actamat.2019.01.020.
[17] J. Kappacher, A. Leitner, D. Kiener, H. Clemens, V. Maier-Kiener, Thermally activated deformation mechanisms and solid solution softening in W-Re alloys investigated via high temperature nanoindentation, Mater. Des. 189 (2020) 108499, doi:10.1016/j.matdes.2020.108499.
[18] V. Maier, A. Hohenwarter, R. Pippan, D. Kiener, Thermally activated deformation processes in body-centered cubic Cr–how microstructure influences strain-rate sensitivity, Scr. Mater. 106 (2015) 42–45, doi:10.1016/j.scriptamat.2015.05.001.
[19] R. Fritz, D. Wimler, A. Leitner, V. Maier-Kiener, D. Kiener, Dominating deformation mechanisms in ultrafine-grained chromium across length scales and temperatures, Acta Mater. 140 (2017) 176–187, doi:10.1016/j.actamat.2017.08.043.
[20] Q. Wei, H.T. Zhang, B.E. Schuster, K.T. Ramesh, R.Z. Valiev, L.J. Kecskes, R.J. Dowding, L. Magness, K. Cho, Microstructure and mechanical properties of super-strong nanocrystalline tungsten processed by high-pressure torsion, Acta Mater. 54 (2006) 4079–4089, doi:10.1016/j.actamat.2006.05.005.
[21] V. Maier, C. Schunk, M. Göken, K. Durst, Microstructure-dependent deformation behaviour of bcc-metals - indentation size effect and strain rate sensitivity, Philos. Mag. 95 (2014) 1766–1779, doi:10.1080/14786435.2014.982741.
[22] C. Bonnekoh, J. Reiser, A. Hartmaier, S. Bonk, A. Hoffmann, M. Rieth, The brittle-to-ductile transition in cold-rolled tungsten sheets: the rate-limiting mechanism of plasticity controlling the BDT in ultrafine-grained tungsten, J. Mater. Sci. (2020) 1–24, doi:10.1007/s10853-020-04801-5.
[23] A.S. Schneider, D. Kaufmann, B.G. Clark, C.P. Frick, P.A. Gruber, R. Mönig, O. Kraft, E. Arzt, Correlation between critical temperature and strength of small-scale bcc pillars, Phys. Rev. Lett. 103 (2009) 105501, doi:10.1103/PhysRevLett.103.105501.
[24] O. Torrents Abad, J.M. Wheeler, J. Michler, A.S. Schneider, E. Arzt, Temperature-dependent size effects on the strength of Ta and W micropillars, Acta Mater. 103 (2016) 483–494, doi:10.1016/j.actamat.2015.10.016.
[25] G.M. Cheng, W.W. Jian, W.Z. Xu, H. Yuan, P.C. Millett, Y.T. Zhu, Grain size effect on deformation mechanisms of nanocrystalline bcc metals, Mater. Res. Lett. 1 (2013) 26–31, doi:10.1080/21663831.2012.739580.
[26] Y. Cui, G. Po, N. Ghoniem, Temperature insensitivity of the flow stress in body-centered cubic micropillar crystals, Acta Mater. 108 (2016) 128–137, doi:10.1016/j.actamat.2016.02.008.

[27] H. Yilmaz, C.J. Williams, J. Risan, B. Derby, The size dependent strength of Fe, Nb and V micropillars at room and low temperature, Materialia 7 (2019) 100424, doi:10.1016/j.mtla.2019.100424.

[28] P. Srivastava, K. Jiang, Y. Cui, E. Olivera, The influence of nano /micro sample size on the strain-rate sensitivity of plastic flow in tungsten, Int. J. Plast. 136 (2021) 102854, doi:10.1016/j.ijplas.2020.102854.

[29] O. Renk, V. Maier-Kiener, I. Issa, J.H. Li, D. Kiener, R. Pippan, Anneal hardening and elevated temperature strain rate sensitivity of nanostructured metals: their relation to intergranular dislocation accommodation, Acta Mater. 165 (2019) 409–419, doi:10.1016/j.actamat.2018.12.002.

[30] J. Kappacher, Controlling the high temperature deformation behavior an thermal stability of ultra-fine grained W by Re alloying, J. Mater. Res. 26 (2020) 1421–1430.

[31] N. Ahmed, A. Hartmaier, Mechanisms of grain boundary softening and strain-rate sensitivity in deformation of ultrafine-grained metals at high temperatures, Acta Mater. 59 (2011) 4323–4334, doi:10.1016/j.actamat.2011.03.056.

[32] A.A. Nazarov, Kinetics of grain boundary recovery in deformed polycrystals, Interface Sci. 8 (2000) 315–322, doi:10.1023/A:1008720710330.

[33] L. Priester, Grain Boundaries: From Theory to Engineering, Springer Science & Business Media, Dordrecht, 2012.

[34] X.C. Liu, H.W. Zhang, K. Lu, Strain-induced ultrahard and ultrastable nanolaminated structure in nickel, Science (80-.) 342 (2013) 337–340, doi:10.1016/j.jallcom.2017.08.018.

[35] Z.B. Wang, S.V. Divinski, Z.P. Luo, Y. Buranova, G. Wilde, K. Lu, Revealing interfacial diffusion kinetics in ultra-fine-laminated Ni with low-angle grain boundaries, Mater. Res. Lett. 5 (2017) 577–583, doi:10.1080/21663831.2017.1368036.

[36] O. Renk, V. Maier-Kiener, C. Motz, J. Eckert, D. Kiener, R. Pippan, How the interface type manipulates the thermomechanical response of nanostructured metals: a case study on nickel, Materialia 15 (2021), doi:10.1016/j.mtla.2021.101020.

[37] J. Chen, E.N. Hahn, A.M. Dongare, S.J. Fensin, Understanding and predicting damage and failure at grain boundaries in BCC Ta, J. Appl. Phys. 126 (2019), doi:10.1063/1.5111837.

[38] D. Scheiber, R. Pippan, P. Puschnig, L. Romaner, Ab initio calculations of grain boundaries in bcc metals, Model. Simul. Mater. Sci. Eng. 24 (2016), doi:10.1088/0965-0393/24/3/035013.

[39] D. Terentyev, F. Gao, Blunting of a brittle crack at grain boundaries: an atomistic study in BCC Iron, Mater. Sci. Eng. A 576 (2013) 231–238, doi:10.1016/j.msea.2013.04.012.

[40] R.L. Smialek, T.E. Mitchell, Interstitial solution hardening in tantalum single crystals, Phil. Mag. 22 (1970) 1105–1127, doi:10.1080/14786437008226921.

[41] R.J. Arsenault, An investigation of the mechanism of thermally activated deformation in tantalum and tantalum-base alloys, Acta Metall. 14 (1966) 831–838, doi:10.1016/0001-6160(66)90003-4.

[42] G.C. Das, R.J. Arsenault, Non-monotonic strengthening in B.C.C. solid solution, Scr. Met. 2 (1968) 495–500, doi:10.1016/0036-9748(68)90181-6.

[43] W. Knabl, G. Leichtfried, R. Stickler, Refractory metals and refractory metal alloys, 2018. doi:10.1007/978-3-319-69743-7_13.

[44] O. Renk, P. Ghosh, R. Pippan, Generation of extreme grain aspect ratios in severely deformed tantalum at elevated temperatures, Scr. Mater. 137 (2017) 60–63, doi:10.1016/j.scriptamat.2017.04.024.

[45] A. Vorhauer, R. Pippan, On the onset of a steady state in body-centered cubic iron during severe plastic deformation at low homologous temperatures, Met. Mater. Trans. A 39 (2008) 417–429, doi:10.1007/s11661-007-9413-1.

[46] F. Wetscher, R. Pippan, Cyclic high-pressure torsion of nickel and Armco iron, Philos. Mag. 86 (2006) 5867–5883, doi:10.1080/14786430600838288.

[47] M.W. Kapp, O. Renk, T. Leitner, P. Ghosh, B. Yang, R. Pippan, Cyclically induced grain growth within shear bands investigated in UFG Ni by cyclic high pressure torsion, J. Mater. Res. 32 (2017) 4317–4326, doi:10.1557/jmr.2017.273.

[48] J.M. Wheeler, J. Michler, Elevated temperature, nano-mechanical testing in situ in the scanning electron microscope, Rev. Sci. Instrum. 84 (2013) 45103, doi:10.1063/1.4795829.

[49] W.C. Oliver, G.M. Pharr, An improved technique for determining hardness and elastic modulus using load and displacement sensing indentation experiments, J. Mater. Res. 7 (1992) 1564–1583, doi:10.1557/JMR.1992.1564.

[50] B.N. Lucas, W.C. Oliver, Indentation power-law creep of high-purity indium, Met. Mater. Trans. A 30 (1999) 601–610, doi:10.1007/s11661-999-0051-7.

[51] V. Maier, K. Durst, J. Mueller, B. Backes, H.W. Höppel, M. Göken, Nanoindentation strain-rate jump tests for determining the local strain-rate sensitivity in nanocrystalline Ni and ultrafine-grained Al, J. Mater. Res. 26 (2011) 1421–1430, doi:10.1557/jmr.2011.156.

[52] W. Köstner, The temperature dependence of the modulus of elasticity of pure metals, Z. Met. 39 (1948).

[53] G. Bérces, N.Q. Chinh, A. Juhász, J. Lendvai, Kinematic analysis of plastic instabilities occurring in microhardness tests, Acta Mater. 46 (1998) 2029–2037, doi:10.1016/S1359-6454(97)00428-X.

[54] N.Q. Chinh, J. Gubicza, Z. Kovács, J. Lendvai, Depth-sensing indentation tests in studying plastic instabilities, J. Mater. Res. 19 (2004) 31–45, doi:10.1557/jmr.2004.19.1.31.

[55] H. Ovri, E.T. Lilleodden, New insights into plastic instability in precipitation strengthened Al-Li alloys, Acta Mater. 89 (2015) 88–97, doi:10.1016/j.actamat.2015.01.065.

[56] H. Ovri, E.T. Lilleodden, On the estimation of thermal activation parameters for portevin-le chatelier effect from nanoindentation data, JOM 71 (2019) 3343–3349, doi:10.1007/s11837-019-03697-0.

[57] V. Maier-Kiener, K. Durst, Advanced nanoindentation testing for studying strain-rate sensitivity and activation volume, JOM 69 (2017) 2246–2255, doi:10.1007/s11837-017-2536-y.

[58] J.M. Wheeler, J. Michler, Invited article: Indenter materials for high temperature nanoindentation, Rev. Sci. Instrum. 84 (2013), doi:10.1063/1.4824710.

[59] A. Bolshakov, G.M. Pharr, Influences of pileup on the measurement of mechanical properties by load and depth sensing indentation techniques, J. Mater. Res. 13 (1998) 1049–1058, doi:10.1557/JMR.1998.0146.

[60] U. Rodrian, H. Schultz, Dislocation relaxation peaks in tantalum, intrinsic and impurity dependent effects, J. Phys. Colloq. 42 (1981) C5–79, doi:10.1051/jphyscol:1981511.

[61] U. Rodrian, H. Schultz, Observations on the Snoek-Koester-relaxation in the system tantalum-oxygen, Z. Met. 73 (1982) 21–29.

[62] J. Baur, W. Benoit, H. Schultz, The dislocation-internal friction peak $\gamma$ in tantalum, Acta Met. 37 (1989) 1159–1166, doi:10.1016/0001-6160(89)90111-9.

[63] F. Qianfeng, The influence of deformation on Snoek peak in Ta-O system, Scr. Mater. 35 (1996) 455–458, doi:10.1016/1359-6462(96)00158-3.

[64] M.S. Blanter, I.S. Golovin, H. Neuhäuser, H.-R. Sinning, Internal Friction in Metallic Materials: A Handbook, Springer, Berlin, Heidleberg, 2007.

[65] S. Nemat-Nasser, R. Kapoor, Deformation behavior of tantalum and a tantalum tungsten alloy, Int. J. Plast. 17 (2001) 1351–1366, doi:10.1016/S0749-6419(00)00088-7.

[66] E. Pink, Thermisch aktivierte Verunreinigungseffekte bei der Verformung von Tantal, Planseebericht Für Pulvermetallurgie 17 (1969) 262–269.

[67] D.H. Lassila, A. Goldberg, R. Becker, The effect of grain boundaries on the athermal stress of tantalum and tantalum-tungsten alloys, Met. Mater. Trans. A 33 (2002) 3457–3464, doi:10.1007/s11661-002-0333-9.

[68] H. Aboulfadl, J. Deges, P. Choi, D. Raabe, Dynamic strain aging studied at the atomic scale, Acta Mater. 86 (2015) 34–42, doi:10.1016/j.actamat.2014.12.028.

[69] M.A. Soare, W.A. Curtin, Solute strengthening of both mobile and forest dislocations: the origin of dynamic strain aging in fcc metals, Acta Mater. 56 (2008) 4046–4061, doi:10.1016/j.actamat.2008.04.027.

[70] E. Rizzi, P. Hähner, On the Portevin-Le Chatelier effect: theoretical modeling and numerical results, Int. J. Plast. 20 (2004) 121–165, doi:10.1016/S0749-6419(03)00035-4.

[71] R. Kirchheim, Metals as sinks and barriers for interstitial diffusion with examples for oxygen diffusion in copper, niobium and tantalum, Acta Meter. 27 (1979) 869–878, doi:10.1016/0001-6160(79)90122-6.

[72] N.L. Peterson, Diffusion in refractory metals, Air Res. Dev. Command., United States Air Force, 1961.

[73] R.W. Powers, M.V Doyle, Diffusion of interstitial solutes in the group V transition metals, J. Appl. Phys. 30 (1959) 514–524, doi:10.1063/1.1702398.

[74] H. Mehrer, Diffusion in Solid Metals And Alloys - Numerical Data and Functional Relationships in Science and Technology, Springer, Berlin, Heidelberg, 1990.

[75] J. Kappacher, A. Leitner, H. Clemens, V. Maier-Kiener, Combination of nanoindentation and microscopy for the examination of aluminum alloys in coarse- and ultrafine-grained condition, Zeitschrift Für Met 56 (2019) 432–442.

[76] K. Durst, V. Maier, Dynamic nanoindentation testing for studying thermally activated processes from single to nanocrystalline metals, Curr. Opin. Solid State Mater. Sci. 19 (2015) 340–353, doi:10.1016/j.cossms.2015.02.001.

[77] S.D. Antolovich, R.W. Armstrong, Plastic strain localization in metals: origins and consequences, Prog. Mater. Sci. 59 (2014) 1–160, doi:10.1016/j.pmatsci.2013.06.001.

[78] K. Leitner (née Babinsky), P.J. Felfer, D. Holec, J. Cairney, W. Knabl, A. Lorich, H. Clemens, S. Primig, On grain boundary segregation in molybdenum materials, Mater. Des. 135 (2017) 204–212, doi:10.1016/j.matdes.2017.09.019.

[79] D. Scheiber, R. Pippan, P. Puschnig, L. Romaner, Ab initio search for cohesion-enhancing impurity elements at grain boundaries in molybdenum and tungsten, Model. Simul. Mater. Sci. Eng. 24 (2016) 85009, doi:10.1088/0965-0393/24/8/085009.

[80] R. Pippan, S. Scheriau, A. Taylor, M. Hafok, A. Hohenwarter, A. Bachmaier, Saturation of fragmentation during severe plastic deformation, Annu. Rev. Mater. Res. 40 (2010) 319–343, doi:10.1146/annurev-matsci-070909-104445.

[81] X. Sauvage, A. Ganeev, Y. Ivanisenko, N. Enikeev, M. Murashkin, R. Valiev, Grain boundary segregation in UFG alloys processed by severe plastic deformation, Adv. Eng. Mater. 14 (2012) 968–974, doi:10.1002/adem.201200060.

[82] G.B. Rathmayr, R. Pippan, Influence of impurities and deformation temperature on the saturation microstructure and ductility of HPT-deformed nickel, Acta Mater. 59 (2011) 7228–7240, doi:10.1016/j.actamat.2011.08.023.

[83] M. Herbig, D. Raabe, Y.J. Li, P. Choi, S. Zaefferer, S. Goto, Atomic-scale quantification of grain boundary segregation in nanocrystalline material, Phys. Rev. Lett. 112 (2013) 1–5, doi:10.1103/PhysRevLett.112.126103.

[84] Z.C. Szkopiak, Oxygen dependence of strain-ageing in niobium, Acta Metall. 16 (1968) 381–391, doi:10.1016/0001-6160(68)90025-4.

[85] J. Crank, The Mathematics of Diffusion, 2nd ed., Oxford university press, Oxford, 1975, doi:10.1021/ja01562a072.

[86] M.G. Cowgill, J. Stringer, The effect of oxygen pressure on the high temperature oxidation of tantalum, J. Less-Common Met. 2 (1960) 233–240, doi:10.1016/0022-5088(60)90017-5.

[87] L.-L. Niu, X. Shu, Y. Zhang, F. Gao, S. Jin, H.-B. Zhou, G.-H. Lu, Atomistic insights into shear-coupled grain boundary migration in bcc tungsten, Mater. Sci. Eng. A 677 (2016) 20–28, doi:10.1016/j.msea.2016.09.029.

[88] O. Renk, R. Pippan, Transition from thermally assisted to mechanically driven boundary migration and related apparent activation energies, Scr. Mater. 154 (2018) 212–215, doi:10.1016/j.scriptamat.2018.05.052.

[89] T.J. Rupert, D.S. Gianola, Y. Gan, K.J. Hemker, Experimental observations of stress-driven grain boundary migration, Science (80-.) 326 (2009) 1686–1690, doi:10.1126/science.1178226.
[90] V. Maier-Kiener, X. An, L. Li, Z. Zhang, R. Pippan, K. Durst, Influence of solid solution strengthening on the local mechanical properties of single crystal and ultrafine-grained binary Cu-AlX solid solutions, J. Mater. Res. 32 (2017) 4583–4591, doi:10.1557/jmr.2017.320.
[91] K. Zhang, J.R. Weertman, J.A. Eastman, Rapid stress-driven grain coarsening in nanocrystalline Cu at ambient and cryogenic temperatures, Appl. Phys. Lett. 87 (2005) 1–4, doi:10.1063/1.2008377.
[92] I.-C. Choi, C. Brandl, R. Schwaiger, Thermally activated dislocation plasticity in body-centered cubic chromium studied by high-temperature nanoindentation, Acta Mater. 140 (2017) 107–115, doi:10.1016/j.actamat.2017.08.026.
[93] D. Brunner, Comparison of flow-stress measurements on high-purity tungsten single crystals with the kink-pair theory, Mater. T. JIM 41 (2000) 152–160, doi:10.2320/matertrans1989.41.152.
[94] H. Li, C. Draxl, S. Wurster, R. Pippan, L. Romaner, Impact of d-band filling on the dislocation properties of bcc transition metals: the case of tantalum-tungsten alloys investigated by density-functional theory, Phys. Rev. B 95 (2017) 94114, doi:10.1103/PhysRevB.95.094114.
[95] D. Tabor, The Hardness of Metals, Oxford University Press, Oxford, 1951.
[96] A. Leitner, V. Maier-Kiener, D. Kiener, Extraction of flow behavior and hall–petch parameters using a nanoindentation multiple sharp tip approach, Adv. Eng. Mater. 19 (2017) 1–9, doi:10.1002/adem.201600669.
[97] X.R. Qian, Y.T. Chou, Grain boundary diffusion of chromium in niobium bicrystals, Philos. Mag. A. 52 (1985) L13–L18, doi:10.1080/01418618508237612.
[98] I. Kair, Y. Mishin, W. Gust, Fundamentals of Grain and Interphase Boundary Diffusion, Wiley, Chichester, 1995.
[99] P. Heitjans, J. Kärger, Diffusion in Condensed Matter - Methods, Materials and Models, Springer, New York, 2005.
[100] D. Hull, D.J. Bacon, Introduction to Dislocations, Butterworth-Heinemann, Oxford, Burlington, 2011.